Magnetic relaxation phenomena and inter-particle interactions in nanosized γ-Fe_2O_3 systems

2003 J. Phys.: Condens. Matter 15 1797

(http://iopscience.iop.org/0953-8984/15/10/325)

INSTITUTE OF PHYSICS PUBLISHING JOURNAL OF PHYSICS: CONDENSED MATTER

J. Phys.: Condens. Matter **15** (2003) 1797–1811 PII: S0953-8984(03)55046-9

Magnetic relaxation phenomena and inter-particle interactions in nanosized γ-Fe_2O_3 systems

D Predoi[1,6], V Kuncser[1], E Tronc[2], M Nogues[3], U Russo[4], G Principi[5] and G Filoti[1]

[1] National Institute for Physics of Materials, RO-76900 Bucharest-Magurele, Romania
[2] Chimie de la Matière Condensée (UA 302), UPMC, 4 Place Jussieu, F-75252 Paris Cedex 05, France
[3] LMOV, CNRS-Université de Versailles, F-78035 Versailles-Cedex, France
[4] Dipartimento di Chimica Inorganica, Metallorganica e Analitica, Università di Padova, via Loredan 2, I-35131 Padova, Italy
[5] Settore Materiali, Dipartimento di Ingegneria Meccanica, Università di Padova and INFM, via Marzolo 9, I-35131 Padova, Italy

E-mail: predoi@cat.mec.pub.ro

Received 22 October 2002, in final form 7 January 2003
Published 3 March 2003
Online at stacks.iop.org/JPhysCM/15/1797

Abstract

Samples of γ-Fe_2O_3 nano-particles with a mean size of 4.0(3) nm and with different hydration and surfactant degrees were prepared by sol–gel methods. Morphology and structural data were obtained by transmission electron microscopy and x-ray diffraction, whereas the surface effects and hyperfine interactions were analysed mainly by Mössbauer spectroscopy. The relative number of surface iron positions was found to be proportional to the amount of OH^- and SO_4^{2-} groups on the particle surface, which in turn is strictly dependent on the preparation conditions. Strong relaxation processes versus temperature were evidenced in the analysed systems. New criteria for the evaluation of the blocking temperature via Mössbauer measurements are proposed. The results are in good agreement with blocking temperatures obtained by magnetic measurements. Moreover, it was shown that the inter-particle magnetic interactions decrease with the number of iron surface states.

1. Introduction

The magnetic behaviour of systems containing fine particles is of valuable interest from both a fundamental and technological point of view. The physical properties of fine particles involve size, shape and surface effects. Ferromagnetic and ferrimagnetic fine particles can be found in magnetic materials of high scientific importance. From the practical point of view, systems of

[6] Author to whom any correspondence should be addressed.

fine magnetic particles are usually used in magnetic inks [1], magnetic fluids [1, 2], magnetic recording [3], permanent magnets [4] and catalysts [5]. In addition, fine magnetic particles occur in many living organisms [6], which make their study essential for the life sciences.

Iron oxides are well known magnetic materials, in particular maghemite, γ-Fe_2O_3, which crystallize in the cubic spinel structure [7, 8]. The γ-Fe_2O_3 nano-particles are used in catalysis or in magnetic recording media. One particular goal of the studies related to fine magnetic particle systems is to determine the smallest size usable for magnetic recording. For each type of material, the magnetic inter-particle interactions, and hence the particle dispersion, are therefore the main characteristics to be controlled. One of the most suitable techniques for preparing ultra-fine spinel ferrite particles in a controlled way is the chemical co-precipitation method [9]. The diameter of the particles can be finally adjusted by subsequent hydro-thermal or annealing treatments [10–12]. Previous investigations have been focused especially on systems of non-aggregated γ-Fe_2O_3 particles [13, 14]. In this work we report on the preparation and characterization of γ-Fe_2O_3 nano-particles with different magnetic interactions among particles.

2. Experimental aspects

The samples have been obtained by oxidation of the colloidal magnetite directly formed in an alkaline medium by co-precipitation of Fe^{II} and Fe^{III} in a stoichiometric ratio of $1/2$. The particle mean size is adjustable in the range from 3 to 11 nm by controlling both the pH and the ionic force of the medium. We have selected the optimal conditions to obtain particles of 4 nm in diameter. The above-formed precipitate of magnetite is oxidized in an acid medium [9] until the Fe^{II}/Fe^{III} ratio falls to 0.05. The resulted sol fractions (30 ml) are further flocculated in two different ways:

(a) by raising the pH up to about 8,

(b) by the rapid addition of 100–150 ml of 1 M H_2SO_4.

In the first case, the surface electrostatic charge of the particles is supposed to vanish, giving rise to a higher aggregation degree and stronger inter-particle interactions. In the second case a surface charge screening is artificially introduced by the specific adsorption of sulfate groups and consequently a lower aggregation degree and weaker inter-particle interactions are expected.

The precipitates were separated and dried at 35 °C, thus producing samples labelled as 4N (case a) and 4S (case b), respectively. Part of sample 4N was additionally dried at 150 °C and has been labelled as sample 4NT.

X-ray diffraction (XRD) measurements were performed using a Philips PW 1380 diffractometer, with Cu Kα radiation, operating in the Bragg–Brentano geometry. Thermogravimetric measurements were performed in order to deduce the charge screening anion contribution at the particle surface. Transmission electron microscopy (TEM) was carried out by using a JEOL 100 CXII microscope. The samples were prepared by evaporating very dilute suspensions onto a carbon-coated grid. Magnetic relaxation phenomena were studied by Mössbauer spectroscopy (MS) and the main results were compared with magnetic measurement data. The Mössbauer spectra were acquired using a constant acceleration spectrometer with symmetrical waveform and a ^{57}Co source (1.4 MBq) in a Rh matrix. Measurements between 4.2 and 300 K have been performed with the sample in a bath cryostat.

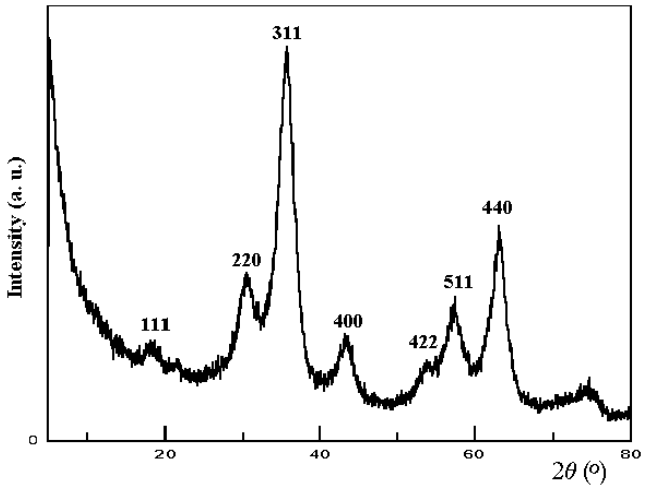

Figure 1. X-ray diffraction pattern of the 4N sample (Cu Kα). A mean coherence length of 3.6(4) nm was derived by using Scherer's formula.

3. Results and discussion

3.1. XRD and TEM studies

Powders of particles with different surface chemical states and different spacing but with the same size distribution were obtained with the above-mentioned preparation procedure. XRD and TEM performed on these samples showed basically similar results.

For example, the XRD profile of the 4N sample evidences very broad lines, reflecting a spinel structure with a unit cell parameter of 8.35 Å (figure 1). A mean coherence length (supposed to approximate the nano-particle mean size) of 3.6(3) nm was deduced from the six diffraction peaks shown in figure 1 by using Scherer's formula. The full widths at half maximum (FWHM) of the peaks were determined from Gaussian profile fits using a Philips PC-APD program. The instrumental effects were removed. The grain size was obtained from the intercept of the linear function $B\cos\theta$ versus $\sin\theta$ [15]. Insignificant slopes were obtained for these linear dependencies, proving almost no strain contributions to the diffraction linewidths.

TEM observations were performed on very dilute sol samples evidencing spherical nano-particles. The particle size distribution was obtained by measuring the diameter of about 500 particles on the micrograph. The diagram of the size distribution for sample 4N is shown in figure 2. A mean diameter of 4.1(4) nm was derived numerically from this distribution. This value is a few per cent higher than that deduced from the XRD data, but the difference may be easily explained by the physical meaning of the quantities derived by the two experimental techniques (coherence length by XRD and physical size by TEM). Therefore, a typical mean diameter of 4.0 nm will be considered in the following.

3.2. Mössbauer studies

3.2.1. A brief overview. Combined magnetic and MS measurements may properly study the magnetic properties of systems consisting of small particles. Theoretical concepts specific to ultrafine particle magnetism [16–20] need to be applied. For nanocrystals less than 20–30 nm, the anisotropy energy KV, with K the magnetic anisotropy energy constant and V the

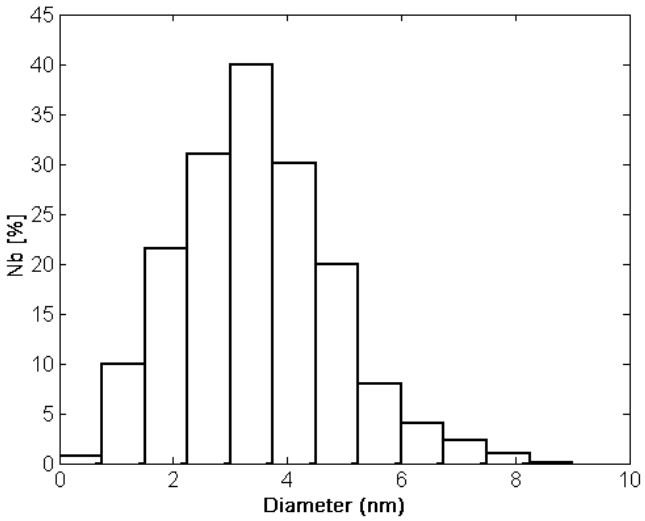

Figure 2. Size distribution obtained from the TEM micrograph of 4N sample. A mean particle diameter of 4.1(4) nm was derived from this distribution.

volume of the particle, becomes comparable with the ambient thermal energy $k_B T$. Therefore, the magnetic properties of non-interacting fine particles are imposed by the thermally driven fluctuations of the ordered magnetic system within the nanocrystal. For a particle with uniaxial anisotropy, the energy $E(\theta)$ required for changing the direction of the total spin by an angle θ from the magnetic easy axis is given by:

$$E(\theta) = KV \sin^2 \theta. \tag{1}$$

The theoretical treatment of the thermally induced fluctuations is usually divided into two regimes, depending on the ratio $r = k_B T/KV$: (i) the regime of the collective excitations, for $r < 0.1$ and (ii) the regime of the superparamagnetic relaxation, for $r > 0.1$. In the first case the coupled spins per particle fluctuate their directions by small angles θ around the magnetic easy axis, leading to an almost linear decrease of the hyperfine field with temperature. In the superparamagnetic relaxation regime, the spins fluctuate by $\theta = 180°$ with a fluctuation time, τ, given in the simplest Néel's model by [21]:

$$\tau = \tau_0 \exp\left(\frac{KV}{k_B T}\right). \tag{2}$$

Actually, the behaviour of a spin-dependent parameter depends on the value of τ as compared to the characteristic measurement time, τ_m. If $\tau \ll \tau_m$, the magnetic relaxation appears so fast that the particle system behaves as a paramagnet, with a giant spin per particle (the superparamagnetic regime), whereas for $\tau \gg \tau_m$ the relaxation appears so slow that quasi-static properties are observed (the blocked regime). The temperature at which $\tau = \tau_m$ is defined as the blocking temperature, T_B, and therefore T_B is relative to τ_m. In spite of the clear phenomenological definition of the blocking temperature, different procedures for finding the experimental temperature where $\tau = \tau_m$ are proposed, depending on the experimental technique. MS is characterized by a quite short characteristic time window, τ_M, in the range of 10^{-9}–10^{-8} s [16–20]. For a given nano-particle size, the fluctuating time decreases with the temperature (see (2)) and consequently the Mössbauer spectrum presents a hyperfine field averaged to zero as soon as the spin fluctuating time becomes much shorter than the Mössbauer

sensing time. In an appropriate regime of temperatures (corresponding to τ not far away from τ_M) the Mössbauer sextet which characterizes a magnetic position will present a collapsing behaviour. The blocking temperature as obtained from Mössbauer spectra taken at different temperatures is proposed to coincide with the temperature where the non-collapsed part of the spectrum (sextet) equals the already collapsed one (doublet or singlet). As will be seen in the following, the blocking temperature deduced by this criterion is subjected to large errors due to the unsuitable fitting procedures in the intermediate relaxation regime.

Another important point is that inside real fine particle assemblies there are usually magnetic inter-particle interactions. RKKY- or superexchange-type interactions could be dominant, depending on the nature of the particles and of the matrix in which these are dispersed. Magnetic dipolar interactions are always present and are usually dominant in powder-type samples. Two possible effects of the inter-particle interactions have to be mentioned: (i) the maintenance of a superparamagnetic state, if the relaxation of each particle is still governed by an anisotropy barrier, E_B, modified by the inter-particle interactions, and (ii) the apparition of a collective state, if only the energy relative to the particle assembly, E_{coll}, may be defined. For a dipolar type dominant interaction, the relaxation phenomena are described in the first case by a modified blocking temperature, and in the second case by a spin freezing temperature, due to both size distribution and disorder of the nano-particles. Moreover, for such interactions, the blocking temperature is supposed to increase versus the interaction strength almost similarly to the freezing temperature [19] and therefore no suppression of the blocked state is expected for a high enough blocking temperature in the non-interacting case (the freezing temperature goes down to zero for non-interacting particle systems).

An overall blocking temperature can also be estimated via magnetic measurements, as being close to the temperature at which the zero field cooled (ZFC) magnetization curve reaches its maximum, T_{max}. For particle systems with size distribution, the ZFC–FC branching temperature (T_{bra}) is related to the blocking temperature of the largest particles, whereas the saturation of the FC magnetization curve depends on the blocking temperature of the finest one. The $R = T_{max}/T_{bra}$ ratio is lower than 1 and it was proved experimentally that it tends to 1 by increasing the magnetic interactions among nano-particles [22].

Mössbauer spectra of the analysed samples, obtained at different temperatures, are shown in figure 3 (sample 4N), figure 4 (sample 4NT) and figure 5 (sample 4S). For samples 4N (figure 3) and 4NT (figure 4) the low temperature spectra showed evidence only of broad sextets, whereas an additional central doublet is present in the low temperature spectrum of sample 4S. By increasing the temperature the magnetic patterns disappear gradually. Therefore, for the analysed samples a relaxation behaviour over a large temperature interval has to be mentioned.

3.2.2. Surface iron states. Useful information about the phase composition in each sample can be obtained from the Mössbauer spectra in the quasi-static regime, namely the spectra collected at very low temperatures. For all samples, these spectra show a broad magnetic sextet with a hyperfine field around 52 T and an isomer shift of 0.5 mm s^{-1}, which are typical for a defected γ-Fe_2O_3 phase. The 7.2 K spectrum of sample 4S shows additionally a paramagnetic phase represented by a doublet with high quadrupole splitting, QS $\approx$ 1.2 mm s^{-1}, and isomer shift, IS $\approx$ 0.9 mm s^{-1}. These values show evidence for the presence of additional Fe^{2+} ions in the 4S sample. Taking into account the preparation conditions for this sample, the paramagnetic doublet has to be assigned to iron positions sensing S neighbours, namely to an Fe sulfate or an Fe sulfide phase. By the hyperfine parameters and the magnetic behaviour at low temperature, all the Fe sulfides and Fe sulfates excepting $[Fe(SO_4)_2]^{2+}$ (which is characterized by IS $\approx$ 0.5 and QS $\approx$ 1.1 mm s^{-1} at 80 K) must be ruled out [23]. Only 12% of the total iron belongs to this phase as deduced from Mössbauer data.

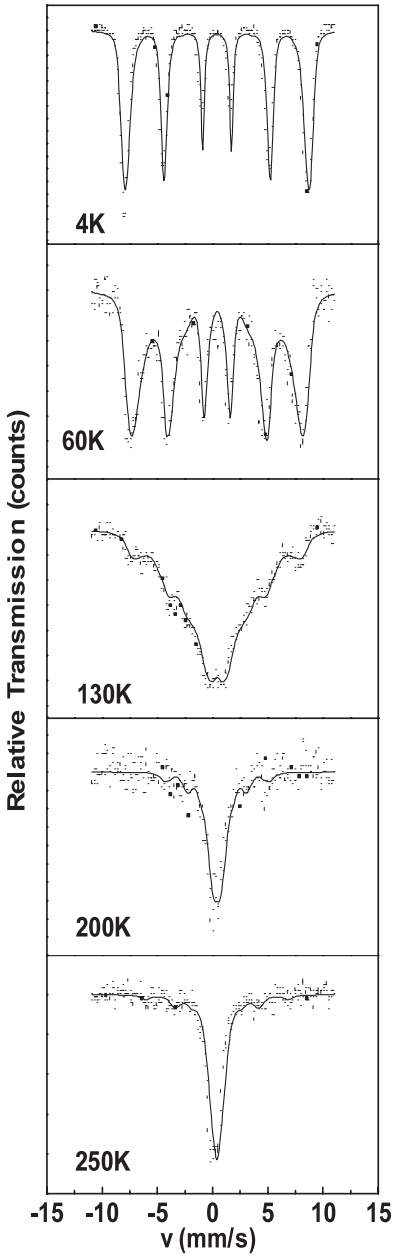

Figure 3. Mössbauer spectra of sample 4N taken at different temperatures.

Even in the static regime, the maghemite sextets are very broad, suggesting a size distribution of the nano-particles. Therefore, all the low temperature Mössbauer spectra were fitted by a distribution of hyperfine fields, following the Hesse–Rubartsch algorithm. The hyperfine field distributions corresponding to the spectra collected at the lowest temperature for each sample are presented in figure 6. At a glance of figure 6, one can observe that the hyperfine field distributions consist in a main lobe centred at about 52 T, and less significant probabilities in the range between 35 and 47 T. Due to the log normal type of the particle

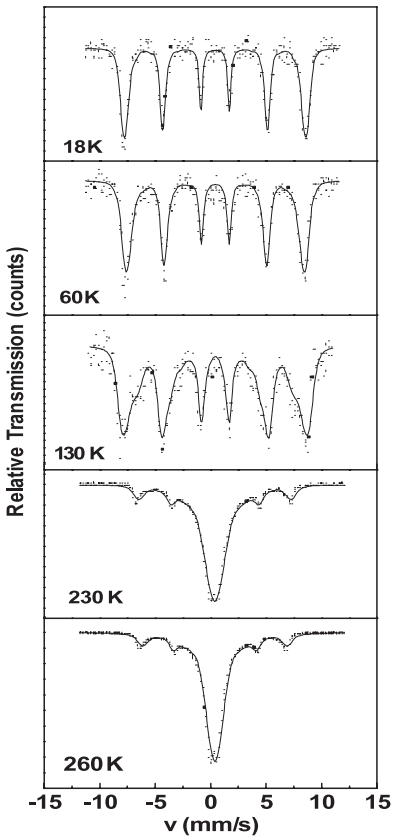

Figure 4. Temperature-dependent Mössbauer spectra of sample 4NT.

size distribution evidenced by electron microscopy and considering that, at these temperatures the iron magnetic moments are blocked, the distribution tail at lower fields has to be due to different Fe configurations in the particle. (It is worth mentioning that the inter-particle interactions could affect the hyperfine field distributions mainly by a small shift toward higher fields.) Therefore, we assumed that the main peak of the probability distribution corresponds to iron in the particle core, whereas the lower hyperfine fields were assigned to surface iron states. Reminding us again of the preparation conditions, the above surface states have to correspond to iron ions sensing the hydroxyl groups (OH^-), which were not removed by the drying procedure.

The maxima of the hyperfine field distributions of figure 6 decrease continuously from sample 4NT to sample 4S, whereas the width distribution increases continuously. A rough evaluation of the main lobe area by the product $P_{max} \cdot W_{1/2}$, where $P_{\max}$ is the maximum probability and $W_{1/2}$ is the width at half maximum, leads to values of 0.92(2) for sample 4NT, 0.84(2) for sample 4N and 0.79(2) for sample 4S (the probability distribution is normalized to 1). Correspondingly, sample 4NT contains only 8(2)% surface iron (sensing OH^- groups), whereas samples 4N and 4S contain 16(2) and 21(2)%, respectively, of the total magnetic ions. Sample 4S contains, in addition, 12% of surface paramagnetic iron sensing SO_4^{2-} groups, and therefore the normalized amount of magnetic iron atoms sensing OH^- groups is only 19(2)%. Because the magnetic state of the surface iron is characterized by much lower magnetic fields (moments) it may influence drastically the magnetic inter-particle interactions.

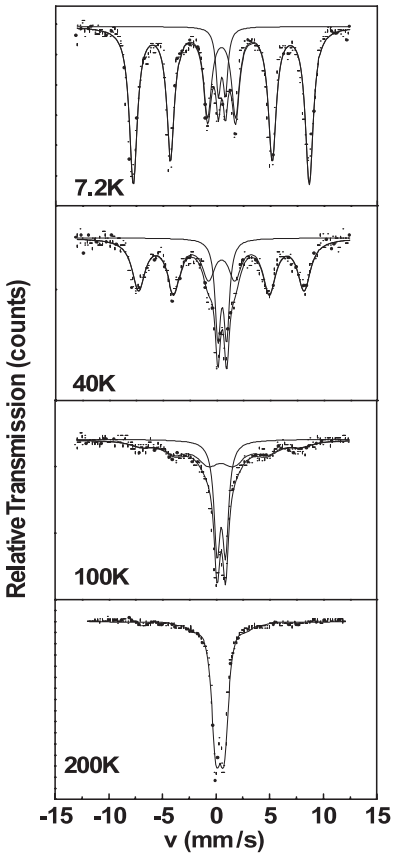

Figure 5. Mössbauer spectra of sample 4S taken at several temperatures.

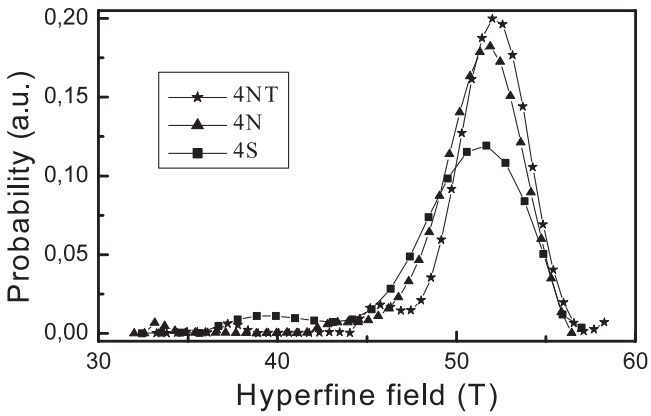

Figure 6. Hyperfine field distributions of the analysed samples in the frozen magnetic regime.

Additional information about the iron surface state has been obtained from the thermogravimetric analysis (TGA). The TGA curves show that sample 4N loses water in two steps: one below 150 °C and the second between 150 and 300 °C. Consequently, sample

Table 1. The relative loss of mass evidenced by the TGA analysis.

Sample	M_{H_2O} (wt%)	M_{SO_3} (wt%)
4NT	3.50	—
4N	7.84	—
4S	9.00	17.8

Table 2. A comparison between the relative number of surface molecules and surface iron positions.

Sample	g_1 (%)	g_2 (%)	r_1 (%)	r_2 (%)
4NT	17	—	8	—
4N	35	—	16	—
4S	42	19	19	12

4N loses OH^- groups (via elimination of water) during the whole thermal treatment, whereas for sample 4NT it happens only above 150 °C. Compared with sample 4N, sample 4S presents an additional endothermic peak (before the transition γ-$Fe_2O_3 \rightarrow \alpha$-$Fe_2O_3$ taking place at 500 °C) corresponding to the loss of SO_3 (via elimination of SO_2 gas [24]). The relative loss of mass (in wt%) corresponding to the analysed samples is presented in table 1.

The ratio between the number of H_2O or SO_3 groups and the number of Fe atoms in each particle, namely g_i, with $i = 1$ for H_2O and $i = 2$ for SO_3, can be easily derived by the formula

$$g_i = n_i/n_{Fe} = 1/2(m_i/m_{\gamma-Fe_2O_3})^*(M_{\gamma-Fe_2O_3}/M_i) \tag{3}$$

where 'i' labels either H_2O or SO_3 and the factor $1/2$ is related to 2 Fe atoms/fu of γ-Fe_2O_3.

The ratios, g_i, deduced by TGA analysis, and the relative fraction of iron surface states, r_i, obtained by MS (with r_1 sensing OH^- and r_2 sensing SO_4^{2-}), are given in table 2. It is worth mentioning that both r_i and g_i are related to the total number of Fe ions per mean sized particle.

It can be observed that for a mean sized particle the relative amount of Fe surface states, r_1, increases almost linearly with the relative amount of water molecules, g_1, with a proportionality factor of about 2 H_2O molecules per surface Fe atom. This result demonstrates that the iron surface states are related to the iron atoms sensing the surface hydroxyl groups and shows that, on average, one surface Fe atom is related to four OH^- groups (two hydroxyl groups giving rise to a water molecule and an additional oxygen still bonded to Fe). The same table occurs for almost two sulfur ions influencing one surface Fe atom, in agreement with the presence of $[Fe(SO_4)_2]^{2-}$ groups at the particle surface.

3.3. Magnetic relaxation

Among other advantages, MS is one of the most suitable methods for spin dynamics investigations. However, in spite of the simple definitions related to such phenomena, e.g. the blocking temperature, there are some major limitations concerning a proper fitting of the Mössbauer spectra in the magnetic relaxation regime. The theories of relaxation behaviour of Mössbauer spectra were developed a long time ago by Blume *et al* (stochastic treatment, e.g. [25]) and Afanas'ev *et al* (perturbation treatment, e.g. [26]). A rapid development of the corresponding methodologies, especially for the stochastic treatment, which is more suitable for a matrix-based analysis, took place over the last decade (see e.g., [27, 28]). Unfortunately, all these methods offer only improved mathematical treatments for the simplest case of Fe positions characterized by discrete hyperfine parameters relaxing with a certain relaxation time. In practice, such methods do not fit a distribution of relaxation times. In fact, nano-

particles in real systems show broad size distributions and consequently their behaviour versus temperature involves relaxation time distributions. For such systems, the relaxation spectra cannot be fitted by using suitable lineshapes, therefore different approaches are necessary. The usual approach is to fit the collapsing spectra with a superposition of Lorentzian sextets (corresponding to the quasi-static regime) and, respectively, singlets/doublets (corresponding to the dynamic regime). In a set of temperature-dependent Mössbauer spectra, the blocking temperature is taken, as previously mentioned, as the temperature where the singlets'/doublets' relative area equals the sextets' relative area. However, due to the improper fitting procedure (none of these theoretical lineshapes are suitable for the intermediate relaxation regime), serious errors occur in deriving the Mössbauer blocking temperature by this criterion. Therefore, in the following we propose new criteria for a better evaluation of the blocking temperature from the Mössbauer spectra. The starting idea is that a distribution of relaxation times requires a distribution of hyperfine fields, which changes continuously with temperature. Consequently, the relaxation behaviour has to be directly related to the variation of this distribution with temperature. The main problem remains to correlate the blocking temperature with a drastic change in the field distribution. Such aspects will be discussed further.

The Mössbauer spectra collected at various temperatures were fitted with a distribution of hyperfine fields following the Hesse–Rubartsch algorithm. The distributions obtained at different temperatures are shown in figures 7(a)–(c) for samples 4N, 4NT, and 4S, respectively. By increasing the temperature, the very pronounced peak initially present at low temperatures becomes broader and moves towards lower fields. At a certain temperature a very unshaped distribution is evidenced, whereas at higher temperatures a new peak at very low fields is well defined. Correspondingly, we can relate the peak at larger hyperfine fields to the magnetic pattern and the contribution at very low fields to the collapsed central component. The transition from the blocked to the relaxed regime, and hence the blocking temperature, may therefore be defined by following the temperature dependence of three typical parameters related to the field distribution: (i) the distribution width, (ii) the intensity of the main peak and (iii) the evolution of the mean hyperfine field. From figures 7(a)–(c) it may be observed that both the distribution width and the intensity of the main peak show a non-monotonic trend versus temperature. The mean hyperfine field decreases drastically in a narrow range of temperatures. The blocking temperature, as related to a specific influence of the spin dynamics on the Mössbauer pattern, has to be suitably defined in relation to the slope discontinuity or inflection points in the temperature dependence of the above-mentioned parameters.

The dependencies of the distribution width and of the intensity of the main peak versus temperature are presented in figures 8 and 9, respectively, for each of the analysed samples. It may be observed that the temperature at which the distribution width reaches its maximum is, in fact, a discontinuity point in the first derivative, because the slopes on the left and right sides are, respectively, opposite in sign and significant in value. The same conclusion might be drawn for the experimental points where the intensity of the mean peak is minimized.

Values of 95(5), 125(5) and 165(5) K can be derived for the blocking temperature of samples 4S, 4N and 4NT, respectively, by assuming that these are related to the discontinuity points in the first derivative of the dependencies presented in figures 8 and 9.

The evolutions of the mean hyperfine field versus temperature are presented in figure 10 for all analysed samples. The curves present a sigmoidal-like decrease with a sharp variation within a narrow temperature range. Taking into account the definition of the blocking temperature relative to the temperature-dependent Mössbauer spectra, we consider that the inflection points in the mean hyperfine field dependencies represent a very good approximation of the blocking temperatures in the MS window time. Mathematically, the inflection points can be exactly deduced from the extreme points in the first derivative of the initial curve. The first derivatives

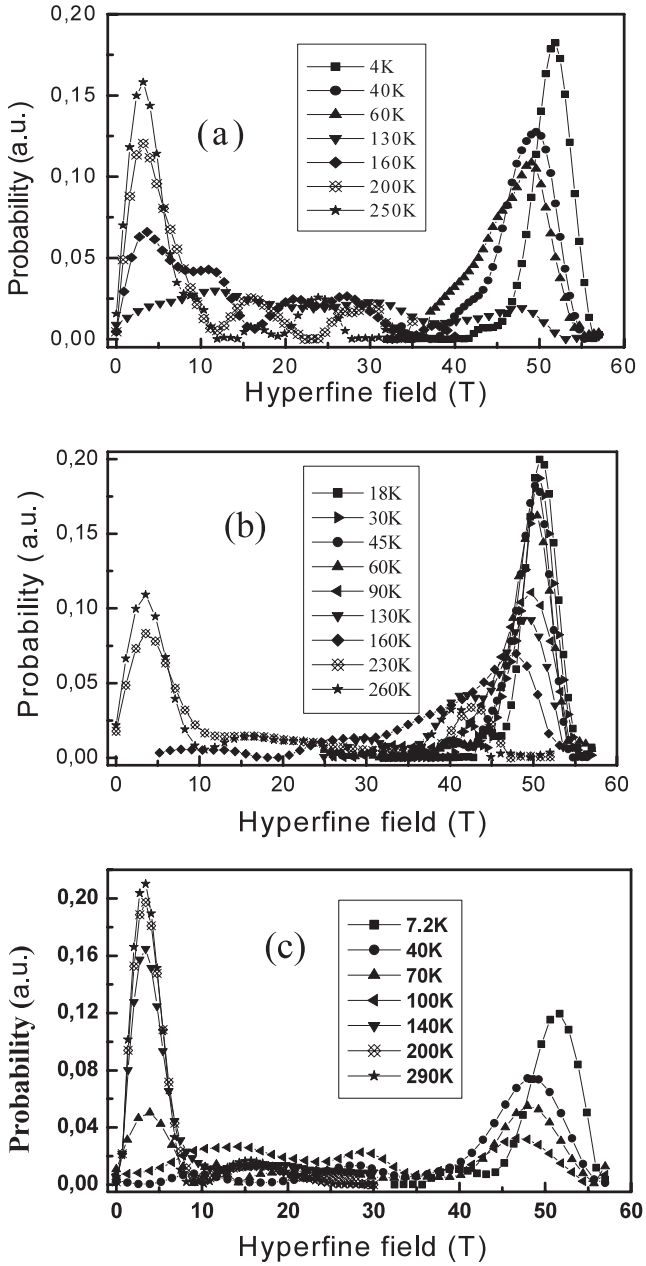

Figure 7. Temperature-dependent hyperfine field distributions for sample 4N (a), sample 4NT (b) and sample 4S (c).

of the mean hyperfine field are presented in the inset of figure 10. Blocking temperatures of 90(5), 110(5) and 180(5) K are obtained for samples 4S, 4N and 4NT, respectively, in acceptable agreement with the previously mentioned values. It is worth mentioning that the blocking temperatures obtained with this last method should be more precise, being derived by fitting the experimental points with much more suitable theoretical dependencies.

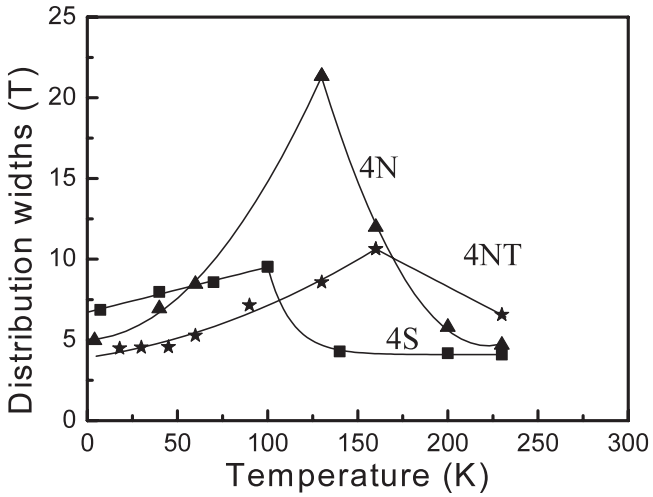

Figure 8. Distribution widths versus temperature in the analysed samples.

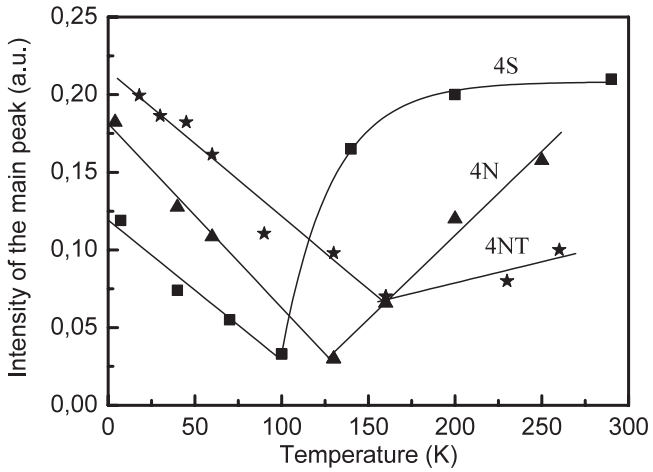

Figure 9. Intensity of the main peak in the hyperfine field distribution versus temperature.

Magnetic measurements performed on the same samples [29] gave the maximum of the ZFC curve values of 89(3), 108(3) and 146(3) K, respectively, in quite good agreement with the Mössbauer results, if the different time windows of the two methods are taken into account.

It may be observed that the derived blocking temperatures are increasing from sample 4S to 4NT, in spite of similar nano-particle mean size and size distributions observed by XRD and TEM, respectively. Therefore, this effect is supposed to be due to different inter-particle interactions in the analysed systems. In order to go more inside this aspect, the effective anisotropy constants were derived starting from relation (2) and the definition of the blocking temperature in MS:

$$K_{eff} = (k_B T_B / V) \ln(\tau_M / \tau_0). \tag{4}$$

By taking $\tau_M = 5 \times 10^{-9}$ s and $\tau_0 = 10^{-11}$ s [17–20] and considering a mean of the above mentioned blocking temperatures obtained in different ways by MS, values of 2.5×10^5, 3.1×10^5 and 4.2×10^5 J m^{-3} can be derived for the anisotropy constant of samples 4S,

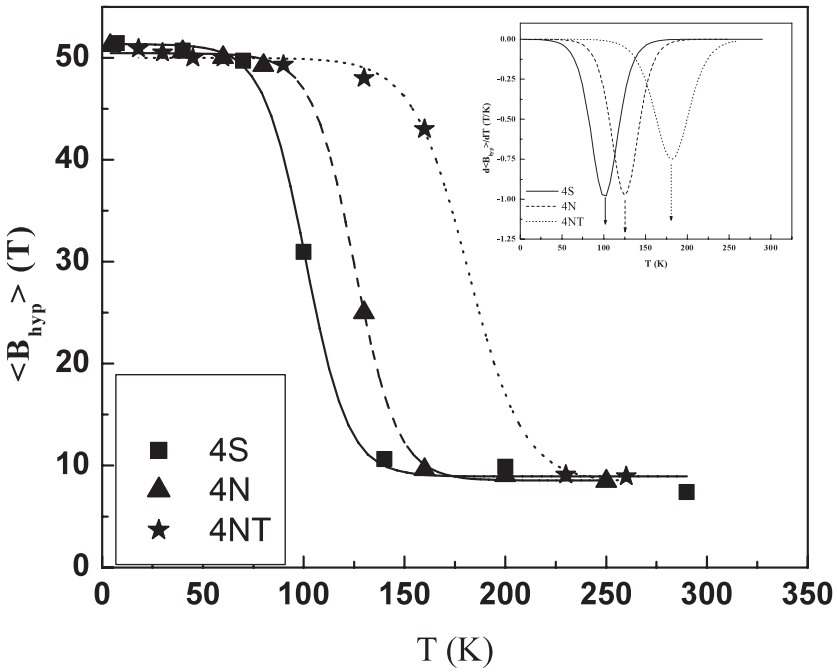

Figure 10. Evolution of the hyperfine magnetic field with temperature in the analysed samples. The derivative of the hyperfine field is shown in the inset. The blocking temperature corresponds to the minimum of the derivative.

4N and 4NT, respectively. These values are several times higher than the bulk anisotropy constant of γ-Fe_2O_3. Since the analysed system consists of maghemite powders, inter-particle dipolar interactions are mainly expected. Therefore, the above values represent the effective anisotropy constants including also the effect of the inter-particle dipolar magnetic interactions. The magnetic energy considered as equating $K_{eff}V$, with K_{eff} the effective overall anisotropy constant, may be in fact expressed as:

$$E = K_u V + E_{int} = (K_u + E_{int}/V)V = K_{eff}V, \tag{5}$$

where K_u is the real anisotropy constant and E_{int} is the inter-particle interaction energy. Assuming that the systems studied have particles with similar dimensions and structures, and consequently almost the same real anisotropy constant, a higher K_{eff} means, in fact, a higher magnetic interaction energy among nano-particles. The present results show that the strongest inter-particle interactions appear in sample 4NT and the lowest in sample 4S.

The magnetic measurements performed on samples 4S, 4N and 4NT give, for the branching temperature (T_{bra}) of the ZFC and FC curves, values of 148, 159 and 185 K, respectively [30]. The ratio $R = T_{max}/T_{bra}$ becomes 0.60, 0.68 and 0.79, respectively, and stands also for the strongest interactions in sample 4NT and the lowest in sample 4S (the stronger the interactions are, the closer to 1 becomes the ratio R), in agreement with the Mössbauer results. The plot of the overall anisotropy constants versus R shows a quite linear dependence (figure 11). Assuming the dependence $E_{int} = f(R)$ and the same particle mean volume in the samples, it results from (5) that $K_{eff} = K_u + cf(R)$, with $c = 1/V = \text{constant}$. A linear dependence of K_{eff} versus R becomes possible only if $E_{int} \sim R$. It may be concluded that, for the range of analysed inter-particle interaction strengths, the interaction energy depends linearly

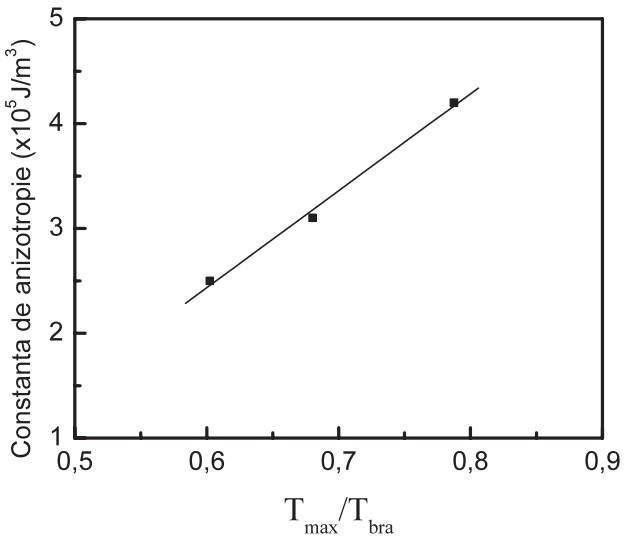

Figure 11. Effective overall anisotropy constants of the analysed samples obtained via MS versus the ratio R obtained by magnetic measurements.

on T_{max}/T_{bra} and the dominant effect of the interactions is to increase the anisotropy energy per particle.

If one takes into account that sample 4S presents the highest number of surface positions and sample 4NT the lowest one, it results in an inverse relation between the number of surface positions and the inter-particle interaction strength. With increasing number of surface magnetic states, characterized by much lower magnetic moments, the inter-particle interactions become weaker. Consequently, sample 4S with around 30% of surface iron positions, related to both HO^- and S^- neighbours, shows the weakest interactions, whereas sample 4NT, treated at 150 °C and with only 6% surface iron, presents the strongest interactions.

4. Conclusions

The magnetic properties of the γ-Fe_2O_3 nano-particles with a mean size of 4.0(3) nm are dominated by the surface magnetic states. Strong relaxation effects were shown below room temperature. The inter-particle magnetic interactions decrease with the number of iron surface states.

The amount of surface iron atoms with low magnetic moments is related to OH^- and SO_4^{2-} groups induced on the nano-particle surface by the preparation conditions.

New criteria were used for the evaluation of the blocking temperatures from Mössbauer data. A pretty good agreement between blocking temperature values obtained by magnetic and Mössbauer measurements was obtained.

In the analysed systems, the dipolar magnetic interactions cannot suppress the transition from the superparamagnetic to the blocked state, the only effect being an increase of the mean anisotropy energy per particle.

Acknowledgments

We express our gratitude to Professor J P Jolivet from Pierre et Marie Curie University for allowing us to use the experimental facilities of his department. We wish also to thank Professor V V Grecu and M N Grecu for fruitful discussions. The financial support by the grant 'Surface influence on the magnetic behaviour of maghemite nano-particles' is gratefully acknowledged by DP. The authors also wish to thank the 'Ministerul Educatiei si Cercetarii', Romania, and 'Ministero degli Affari Esterri', Italy, for their joint financial support by the XIIIth Romania-Italy Scientific Protocol, positions 9 and 23.

References

[1] Charles S W and Popplewell J 1980 *Ferromagnetic Materials* vol 2, ed E P Wohlfarth (Amsterdam: North-Holland) p 509
[2] Berkovsky B (ed) 1977 *Thermomechanics of Magnetic Fluids* (London: Hemisphere) p 111
[3] Bate G 1981 *J. Appl. Phys.* **52** 2447
[4] Zijlstra H 1982 *Ferromagnetic Materials* vol 3, ed E P Wohlfarth (Amsterdam: North-Holland) p 107
[5] Haneda K 1987 *Can. J. Phys.* **65** 1233
[6] Frankel R B and Blakemore R B 1980 *J. Magn. Magn. Mater.* **15–18** 1562
[7] Morrish A H 1980 *Growth, Properties, and Applications* ed H C Freyhardt (Berlin: Springer) p 171
[8] Bate G 1980 *Ferromagnetic Materials* vol 2, ed E P Wohlfarth (Amsterdam: North-Holland) p 381
[9] Jolivet J P, Fruchart J M and Massart R 1983 *Nuov. J. Chem.* **7** 325
[10] Tronc E and Jolivet J P 1988 *J. Physique* **49** C8 1823
[11] Tronc E and Jolivet J P 1992 *Magnetic Properties of Fine Particles* ed J L Dormann and D Fiorani (Amsterdam: North-Holland) p 199
[12] Jolivet J P and Tronc E 1988 *J. Colloid Interface Sci.* **125** 688
[13] Tronc E, Préne P, Jolivet J P, d'Orazio F, Lucari F, Fiorani D, Godinho M, Cherkaoui R, Nogues M and Dormann J L 1995 *Hyperfine Interact.* **95** 129–48
[14] Prodan D, Grecu V V, Grecu M N, Tronc E and Jolivet J P 1999 *Meas. Sci. Technol.* **10** L41–3
[15] Suryanarayana C and Grant M 1998 *Norton in X-ray Diffraction; A Practical Approach* (New York: Plenum)
[16] Haneda K 1987 *Can. J. Phys.* **65** 1233
[17] Morup S 1983 *J. Magn. Magn. Mater.* **37** 39
[18] Campbell S J and Gleiter H 1993 *Mössbauer Spectroscopy Applied to Magnetism and Material Science* vol 1, ed G J Long and F Grandjean (New York: Plenum)
[19] Dormann J L, Fiorani D and Tronc E 1997 *Advances in Chemical Physics* vol XCIII, ed I Prigogine and A Rice (New York: Wiley)
[20] Tronc E 1996 *Nuovo Cimento* D **18** 163
[21] Néel L 1949 *Ann. Geophys.* **5** 9
[22] Prene P 1995 Particles d'oxyde de fer spinelle, physico-chemie des dispersions et comportement magnetique *PhD Thesis* Pierre and Marie Curie University
[23] Greenwood N N and Gibb T C 1971 *Mössbauer Spectroscopy* (London: Chapman and Hall) p 134, 284
[24] Dorsey D and Buecker B J 1988 *Compositional Analysis by Thermogravimetry, ASTM STP 997* ed C M Earnest (Philadelphia, PA: American Society for Testing and Materials) pp 254–8
[25] Blume M 1965 *Phys. Rev. Lett.* **14** 96
Blume M and Tjon J A 1968 *Phys. Rev.* **165** 447
Tjon J A and Blume M 1968 *Phys. Rev.* **165** 459
[26] Afanas'ev A M and Kagan Yu 1964 *Sov. Phys.–JETP* **18** 1139
Kagan Yu and Afanas'ev A M 1965 *Sov. Phys.–JETP* **20** 743
[27] Phannes H-D and Magalhas-Paniago R 1994 *Hyperfine Interact.* **173** 79
[28] Dattagupta S 1987 *Relaxation Phenomena in Condensed Matter Physics* (London: Academic)
Dattagupta S 1977 *Phys. Rev.* B **16** 158
Dattagupta S 1977 *Phys. Rev.* B **16** 3893
[29] Prodan D, Chaneac C, Tronc E, Jolivet J P, Cherkaour R, Ezzir A, Nogues M and Dormann J L 1999 *J. Magn. Magn. Mater.* **203** 63
[30] Predoi D, Kuncser V, Nogues M, Tronc E, Joliver J P and Filoti G 2003 *J. Opt. Adv. Mater.* at press